Experimental study on pyrolysis gas products of chlorinated polyvinyl chloride and its smoke properties during combustion

Ang Li[1] · Biqing Huang[2] · Wenlong Zhang[2] · Yanming Ding[2] · Ru Zhou[3]

Abstract

The pyrolysis gas products of chlorinated polyvinyl chloride (CPVC) are first discussed based on thermogravimetry–Fourier transform infrared spectra–mass spectrometry (TG–FTIR–MS) analysis. The results of TG–FTIR preliminarily show that CPVC pyrolysis can be divided into two stages: the main gas products or functional groups are hydrogen chloride (HCl), chlorinated compounds, alkanes, alkenes and aromatic compounds in Stage I, while alkanes, aromatic compounds and alkenes in Stage II. By coupling MS, the main products can be further refined into hydrogen chloride and benzene in Stage I, while homologues, derivatives and polycyclic aromatic compounds of benzene (xylene and ethylbenzene, chlorobenzene and 1-chloronaphthalene, naphthalene and fluorene and so on) in Stage II. Moreover, compared with the pyrolysis gas products of PVC, chlorine is not completely converted into hydrogen chloride, and some of it is converted into other chlorinated compounds. Based on the above results, the possible reactions from molecular structure during CPVC pyrolysis are also put forward. Furthermore, the CPVC combustion properties and smoke production in cone calorimeter experiment are analyzed by the measured mass loss rate, heat release rate, smoke and CO/CO_2 production rate.

Keywords Chlorinated polyvinyl chloride · Pyrolysis · TG–FTIR–MS · Combustion · Cone calorimeter

Introduction

Nowadays, with the popularization of urbanization and the improvement of living standard, plastic products are widely used due to its characteristics of durability, low cost and convenience and so on [1, 2]. Chlorinated polyvinyl chloride (CPVC) is a new type of engineering plastics with broad application prospects. It can be obtained by further chlorination of polyvinyl chloride (PVC). When the PVC is chlorinated, its physical and chemical performance, such as irregularity, polarity, solubility and chemical stability of molecular chain arrangement, can be improved [3]. However, due to the increase in the use of CPVC, the disposal of its waste must be an urgent problem to be solved. As far as waste disposal is concerned, converting it into new energy is a hot topic in the future. Pyrolysis, as a very promising thermochemical technique [4, 5], has been got closely attention by providing an excellent alternative to transform plastic wastes into energy fuels or valuable chemicals, especially decomposing long-chain polymer molecules into smaller, less complex molecules [6]. The pyrolysis recycling of waste thermoplastics such as polyethylene terephthalate (PET), polyethylene (PE), polypropylene (PP), polystyrene (PS) and PVC has been widely studied [1, 7, 8].

The pyrolysis kinetics and reaction model of CPVC have also been described in our previous studies [9]. It should be emphasized that only C and H elements are involved in PE, PP, PS plastics, while the presence of Cl element in CPVC will lead to the production of toxic and harmful gases in the process of thermal degradation. These gases need to be removed or recovered at the right pyrolysis temperature and time in the pyrolysis process. Therefore, it is necessary to study the gas products of CPVC thermal degradation using new research techniques. Thermogravimetric (TG) coupled with other

✉ Biqing Huang
1201820343@cug.edu.cn

✉ Yanming Ding
dingym@cug.edu.cn

[1] College of Power Engineering, Naval University of Engineering, Wuhan 430003, China

[2] Faculty of Engineering, China University of Geosciences, Wuhan 430074, China

[3] Jiangsu Key Laboratory of Urban and Industrial Safety, College of Safety Science and Engineering, Nanjing Tech University, Nanjing 211800, China

techniques, such as Fourier transform infrared spectra (FTIR) and mass spectrometry (MS), is an effective way not only to investigate the thermal behavior, but also to monitor gas products. Furthermore, pyrolysis as part of gasification and combustion processes can help to provide a better understanding and planning of important industrial processes [10, 11]. Kai et al. [12, 13] studied the co-pyrolysis of rice straw and corn stalk with the high density polyethylene (HDPE) blends using TG–FTIR–MS. Chen et al. [14, 15] explored the pyrolysis mechanism and gas products of both ethylene–propylene-diene monomer (EPDM) and waste phenolic fibre-reinforced plastic (FRP) by TG–FTIR–MS. However, to the best of our knowledge, there are quite few studies with respect to the specific gas products of CPVC in the whole pyrolysis process. Therefore, TG–FTIR–MS was firstly used to explore the gas products at the two stages of CPVC. It is valuable for industrial large-scale removal or recovery of chlorinated compounds and aromatic compounds from CPVC pyrolysis.

In addition, plastic products in daily life cannot avoid industrial fire accidents when they are produced or used [16], it is necessary to study its smoke properties during combustion. Cone calorimeter has been widely used to evaluate the fire hazard and investigate the smoke properties of materials. Some typical plastic in the industry have been researched for their combustion characteristics by cone calorimeter experiment, such as PS [2], HDPE and poly(methyl)methacrylate, PMMA [17, 18], epoxy resin/carbon fiber composites [19], PVC [20] and so on. However, the smoke properties of CPVC during combustion have been little studied [21]. Hence, the effect of the external heat flux with the combustion parameters and their correlation are discussed. Meanwhile, the relationship between CPVC combustion heat release and smoke generation was also determined.

As discussed above, the aim of current paper is to explore the gas products during pyrolysis and smoke properties during combustion of CPVC. TG–FTIR–MS was used to confirm its pyrolysis gas products and predict possible reactions. Cone calorimeter experiment was used to analyze its combustion behaviors including the mass loss rate (MLR), heat release rate (HRR), fire performance index (FPI), fire growth index (FGI), smoke production rate (SPR) and CO, CO_2 production rate. The four different external heat fluxes (35, 50, 65 and 80 kW m^{-2}) were selected according to the heat required by CPVC in the fire. It also determines whether the correlation between the HRR and the SPR was influenced by the external heat fluxes.

Experimental

Materials

The CPVC samples used in this study are produced by the Shenzhen Hong Cheng Plastic Co., Ltd. The product type

of CPVC is N-500. The chlorine content of CPVC sample is 63.85%, and its specific element analysis has been mentioned in our previous study [9].

TG–FTIR–MS experiments

The TG–FTIR–MS experiment was performed using a Perkin Elmer Pyris 1 thermogravimetric analyzer coupled with Frontier FTIR spectroscopy spectrophotometer and a Clarus SQ 8 T mass spectrometer. Before the experiment, about 6 mg powder sample was evenly distributed in a capless alumina cup. The experiment was conducted from 400 to 900 K at 20 K min^{-1} in helium atmosphere with a gas flow rate of 100 mL min^{-1}. The temperature of gas transportation connection between the apparatuses was set to 763 K to ensure the pyrolysis products in a gas state.

Cone calorimeter experiments

Cone calorimeter is an instrument for measuring the combustion parameters of materials and can be used to evaluate the material hazard. It is mainly to test the samples based on the oxygen consumption principle. The external heat flux of the sample mainly comes from the cone heater. The external heat flux is generally adjusted from 0 to 120 kW m^{-2} by the temperature controller. In this study, the cone calorimeter experiment with multiple external heat fluxes including 35, 50, 65 and 80 kW m^{-2} was carried out based on ISO 5660–1 standard [22]. Prior to the experiment, the size of the sample was cut to 100 mm × 100 mm × 6 mm (length × width × thickness). Base on the study of Srivastav et al. [23], the thermal response characteristic of CPVC is constant when the sample thickness is more than 4 mm for both the case of with aluminum and without aluminum. Hence, the sample bottom and sides were covered with aluminum foil to prevent heat loss to the outside. Meanwhile, insulation cotton was placed between the sample and the standard sample box. During the experiment, the sample box was placed horizontally on the lifting platform. By adjusting the lifting platform, the distance between the upper surface of the sample and the heating cone was guaranteed to be 25 mm. MLR and HRR were measured and recorded. The gas smoke generated after the sample combustion was pumped through the gas collection system to the gas smoke measurement and gas analysis device. The gas composition analysis was mainly performed by the CO/CO_2 gas analyzer, and its variation with time was recorded by the data terminal.

Results and discussion

Pyrolysis gas products analysis

TG analysis

The detailed pyrolysis behaviors of CPVC have been investigated in our previous study [9]. Figure 1 shows the mass loss and MLR at 20 K min^{-1} with two obvious stages (marked in green dashed boxes). The two stages are in the temperature range of about 547–627 K and 680–792 K with peak temperature of 585 K and 743 K, respectively.
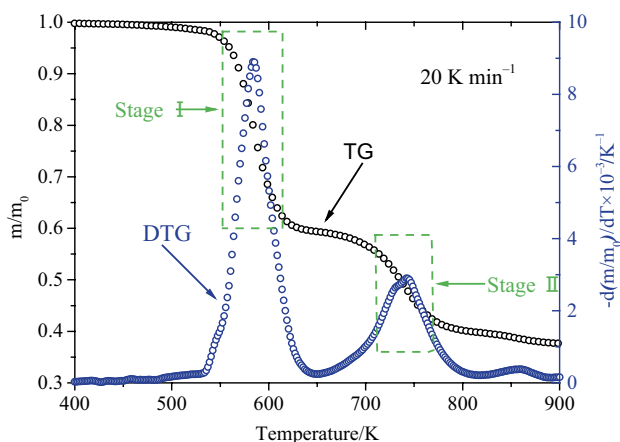

Fig. 1 The pyrolysis curves of TG and DTG at 20 K min^{-1}

TG–FTIR analysis

FTIR coupled with TG was conducted to monitor functional groups and gas products during pyrolysis of CPVC. Considering that CPVC is the product of further chlorination of PVC and the reaction mechanism of CPVC may be similar to that of PVC, the FTIR spectral analysis of CPVC in this paper is also based on the FTIR spectral study of PVC [7, 24–26]. The possible functional groups corresponding to characteristics absorption bands of the FTIR spectra are listed in Table 1.

To further compare the difference of pyrolysis gas in Stages I and II, the FTIR spectra at two peak temperatures (585 K and 743 K) are shown in Fig. 2a. It can be seen that the absorption bands 2400–2250 cm^{-1} of C=O and 3800–3500 cm^{-1} of O–H appear in Stage I, which may be due to the high sensitivity of FTIR to CO_2 and H_2O [27]. In addition, the absorption peaks at 3100–2600 cm^{-1} correspond to H–Cl asymmetrical stretching, which is attributed to the production of hydrogen chloride (HCl). Moreover, the absorption peaks of –CH$_3$ and –CH$_2$– are overlapped with the absorption bands of H–Cl in the 3000–2800 cm^{-1}. Meanwhile, there is an obvious absorption band of 800–600 cm^{-1} in the fingerprint region, which is the characteristic of C–Cl stretching vibration. In the process of dehydrochlorination, the rupture of C–Cl will form C=C corresponding to the absorption band of 1680–1600 cm^{-1} [26]. Due to the high absorption peak of H–Cl and C–Cl, the two absorption bands of 1500–1000 cm^{-1} and 970–670 cm^{-1} (aromatic hydrocarbons) are less noticeable. The above analysis suggests that the main gas products in Stage I of CPVC pyrolysis may be HCl, chlorinated compounds, alkanes, alkenes and aromatic compounds. In Stage II, the absorption band of H–Cl basically disappears, and the most obvious absorption peaks are

Table 1 A summary of IR bonds selected for analysis of functional groups

Functional group	Vibrational mode	Assigned wavenumber/cm^{-1}
H–Cl	H–Cl asymmetrical	2820–2600
C–Cl	Stretching	800–600
C=C	Stretching	1680–1600
C=C (benzene skeleton)	Stretching	1690–1450
=C–H (benzene skeleton)	Stretching	3100–3000
=C–H (benzene skeleton)	Bending	900–700
–CH$_3$, –CH$_2$–	Stretching	3000–2800
–CH$_3$, –CH$_2$–	Bending	1480–1300
Mononuclear aromatic hydrocarbons	Skeletal vibrations	1500–1400
Mononuclear aromatic hydrocarbons	In-plane bending	1300–1000
Aromatic hydrocarbons	Out of plane bending	910–670
O–H	Stretching	3800–3500
C=O	Stretching	2400–2250

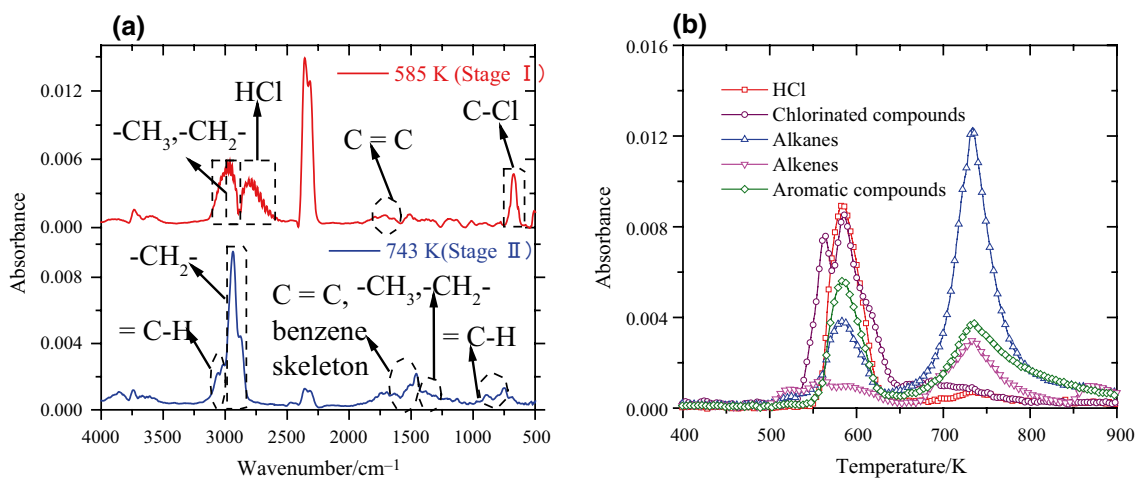**Fig. 2 a** FTIR spectra at typical temperatures in Stages I and II, and **b** typical gas products versus temperature

–CH$_2$–. Instead, two absorption bands of 3100–3000 cm^{-1} and 900–700 cm^{-1} with benzene skeleton =C–H appear. Besides, the bending vibration absorption band of –CH$_3$ and –CH$_2$– (1480–1300 cm^{-1}) can also be observed. It is inferred that the main gas products in Stage II of CPVC pyrolysis should be alkanes, aromatic compounds and alkenes.

In order to better reflect the variation of gas products in the two stages, typical gas products are taken as a function of temperature and shown in Fig. 3b. Zhou et al. [28] analyzed the FTIR spectra of PVC and concluded that the main gas products in the Stage I of pyrolysis were hydrogen chloride, benzene and alkyls, while the second stage was more alkyls and alkenes. However, by comparison with our current study, it is found that the biggest difference of FTIR spectra between CPVC and PVC is the presence of chlorinated compounds in Stage I. Namely, all chlorine during PVC pyrolysis is converted into hydrogen chloride In Stage I, while part of chlorine during CPVC pyrolysis is converted into chlorinated compounds.

MS analysis

It is worth noting that the TG–FTIR results can only reflect the variations of main function groups during pyrolysis, but the exact gas products cannot be identified. Hence, it is necessary of MS analysis to be replenished to establish the specific gas products. Figure 3 shows the total ion chromatogram (TIC) reconstruction of the gas products and the evolution curves of the main ion fragments ($m/z = 36.5, 62, 64, 78, 80, 92, 106, 113.5, 128, 142, 148, 154, 162.5, 166, 178$) during the whole CPVC pyrolysis. Table 2 lists the typical fragmented ions corresponding to the possible gas products.

As shown in Fig. 3a, there are two distinct peak regions in the TIC diagram, which correspond to the two stages of CPVC pyrolysis. For certain gas products, single ion

monitor (SIM) was adopted in the mass detector. Figure 3b shows that the two main gas products in Stage I are HCl ($m/z = 36.5$) and benzene ($m/z = 78$). Meanwhile, the maximum MS signal of HCl is more than 4×10^5, nearly 3.85 times that of benzene, which is consistent with the research results of PVC by Sun et al. [29]. The changes of four main gas products with temperature in Stages I and II are shown in Fig. 3c. For $m/z = 62, 64$ and $78, 80$, it is deduced to be chloroethylene and chloropropane due to the existence of chlorine isotopes (^{35}Cl and ^{37}Cl). Then it means that the chlorine of CPVC pyrolysis is not completely converted to HCl, which is consistent with the results of FTIR spectra. According to the MS of PVC by Knümann et al. [30], the gas products corresponding to $m/z = 128$ and 166 may be polycyclic aromatic hydrocarbons (PAHs) naphthalene and fluorene. Furthermore, the main gas products produced in Stage II are shown in Fig. 3d. For $m/z = 92$ and 148, it is regarded as methylbenzene and amylbenzene, respectively. For $m/z = 106$, it may represent two different homologues of benzene, xylene or ethylbenzene. For $m/z = 113.5$ and 162.5, they could be chlorobenzene and 1-chloronaphthalene, respectively, which also indicates that chlorine in Stage I has not been completely transformed. The most possible gas products for $m/z = 142, 154$ and 178 are PAHs.

Reactions prediction

It is well-known that the main repeating unit of PVC is –CH$_2$–CHCl–. However, since CPVC is obtained by further chlorinating PVC, there are three main types of repeating units in CPVC molecular structure: –CH$_2$–CHCl–, –CHCl–CHCl– and –CCl$_2$– units. The number of these three units is related to the chlorine content. In this study, chlorine content of sample is 63.85%, less than 65%, and then it is referred that the main repeat units of current CPVC are
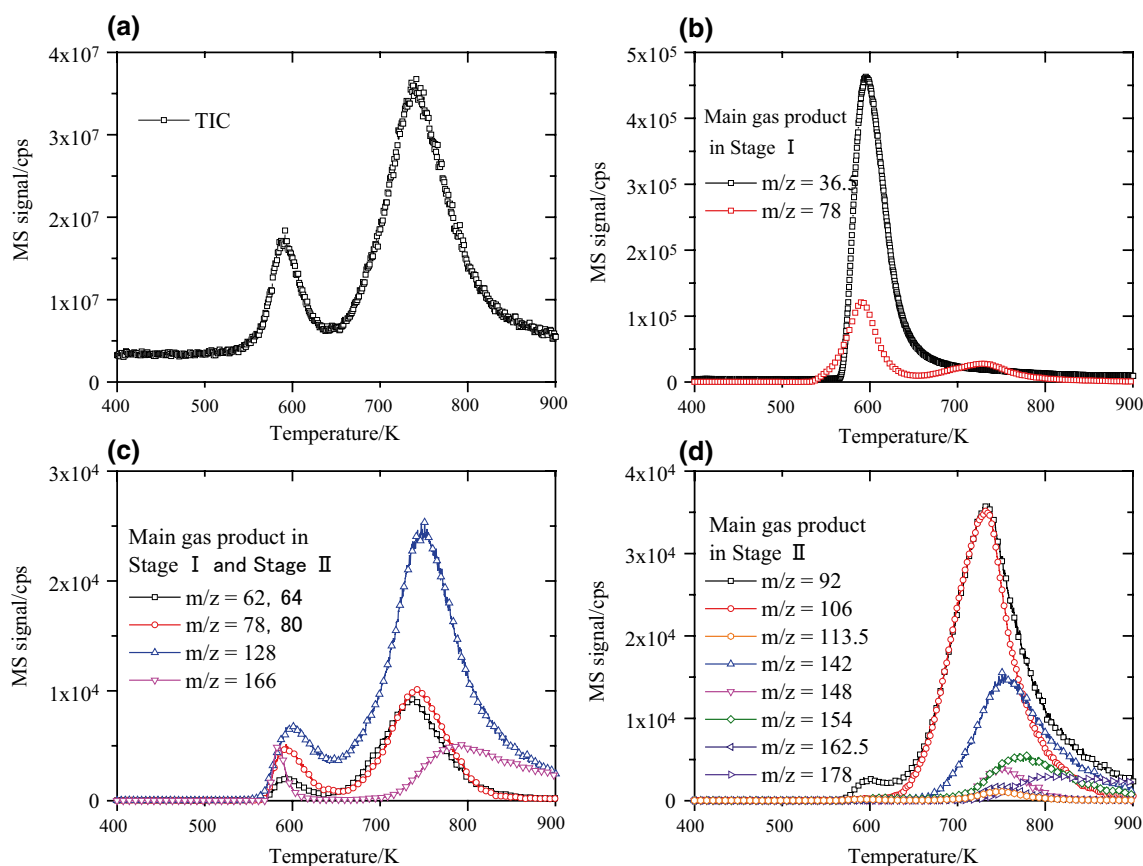
Fig. 3 **a** TIC reconstruction of gas products during pyrolysis, **b** curves of the main ion fragments in Stage I, **c** curves of the main ion fragments in Stages I and II, and **d** curves of the main ion fragments in Stage II

–CH$_2$–CHCl– and –CHCl–CHCl– [31]. Due to the increase of chlorine content, CPVC pyrolysis products at two stages are different from PVC pyrolysis, especially in the transformation of chlorine in the whole process. Therefore, based on the gas products analyzed by TG–FTIR–MS, the possible reactions of CPVC pyrolysis at two stages are shown in Figs. 4 and 5.

In Stage I, the main reactions can be divided into three: First, C–Cl and C–H in repeated –CH$_2$–CHCl– units are broken to form repeated C=C chain structure and generate hydrogen chloride; Second, on the basis of reaction (a), part of repeated C=C chain structure is cycled to form aromatic hydrocarbons; Third, repeated –CHCl–CHCl– units remove hydrogen chloride and produce chlorinated hydrocarbons and some C=C structure containing chlorine.

In Stage II, as the temperature increases, the new reactions will be happened through repeated C=C chain structure and C=C structure containing chlorine. There are four kinds of main reactions in Fig. 5: First, C=C bond breaks to produce large quantities of hydrocarbons; Second, benzene homologues (methylbenzene and xylene, etc.) may be produced when chain C=C is cyclized; Third,

PAHs (such as biphenyl, phenanthrene) can also be produced; Fourth, repeated C=C chain structures containing chlorine can be cyclized to produce chlorobenzene and 1-chloronaphthalene.

Smoke properties analysis during combustion

Mass loss rate

MLR is a important parameters to characterize the fire risk of materials. Figure 6a shows the MLR under four different external heat fluxes (35, 50, 65 and 80 kW m^{-2}). There are two peaks in the whole combustion process. The higher the external heat flux is, the faster the peaks appear. Namely, with the increase of heat flux, the peak position appears earlier. Based on the heat and mass transfer model of thermoplastic solid fuel proposed by Rhodes and Quintiere [32, 33], the transient MLR can be estimated as:

$$\dot{m}'' = \frac{1}{L}\left(\dot{q}_e'' + \dot{q}_{f,c}'' + \dot{q}_{f,r}'' - \dot{q}_{cond}'' - \sigma\left(T_V^4 - T_\infty^4\right)\right), \tag{1}$$

Table 2 The main ion fragments corresponding to the possible gas products

No	m/z	Molecular formula	Possible gas products
1	36.5	HCl	Hydrogen chloride
2	44	C_3H_8	Propane
3	62.64	C_2H_3Cl	Chloroethylene
4	72	C_5H_{12}	Pentane
5	78	C_6H_6	Benzene
6	78.80	C_3H_7Cl	Chloropropane
7	92	C_7H_8	Methylbenzene
8	106	C_8H_{10}	Xylene/ethylbenzene
9	113.5	C_6H_5Cl	Chlorobenzene
10	128	$C_{10}H_8$	Naphthalene
11	142	$C_{11}H_{10}$	Methylnaphthalene
12	148	$C_{11}H_{16}$	Amylbenzene
13	154	$C_{12}H_{10}$	Acenaphthene/biphenyl
14	162.5	$C_{10}H_7Cl$	1-Chloronaphthalene
15	166	$C_{13}H_{10}$	Fluorene
16	178	$C_{14}H_{10}$	Phenanthrene/anthracene
17	202	$C_{16}H_{10}$	Fluoranthene/pyrene
18	218	$C_{16}H_{26}$	Hexadecyl aromatic alkane
19	228	$C_{18}H_{12}$	Chrysene/tetraphene
20	252	$C_{20}H_{12}$	Benzo[b]fluoranthene/benzo(k)fluoranthene/benzo(a)pyrene

where $\dot{m}''$ denotes the transient MLR of the sample, g s^{-1} m^{-2}. L represents the heat of gasification of the sample, kJ g^{-1}. $\dot{q}_e''$ is the external heat flux, kW m^{-2}. $\dot{q}_{f,c}''$ and $\dot{q}_{f,r}''$ are the convective and radiative heat flux from the flame, kW m^{-2}, respectively. $\dot{q}_{cond}''$ denotes the thermal conduction loss from the sample, kW m^{-2}. $\sigma\left(T_V^4 - T_\infty^4\right)$ denotes the surface re-radiation heat loss of the sample, kW m^{-2}. σ is Stefan–Boltzmann constant (5.6704×10^{-8} W m^{-2} K^{-4}). T_V

and T_∞ are the vaporization temperature of the sample, K, and environment temperature, K, respectively.

In the field of engineering, for a given material and specimen size, Rhodes and Quintiere [32] believes that except for the term $\dot{q}_e''$, other terms can be regarded as constants when MLR reaches the moment of peak value or at steady-state combustion. Therefore, the peak and average MLRs may have a linear relationship with the external heat flux. Then Eq. (1) can be reduced as follows:

$$\dot{m}'' = \frac{1}{L}\dot{q}_e'' + C_1, \tag{2}$$

where C_1 is a constant.

The first peak, second peak, and average MLR (PMLR$_1$, PMLR$_2$ and AMLR) values are listed in Table 3. Figure 6b shows the correlation between the three kinds of MLR versus external heat flux. With the increase of heat flux, the first MLR, second MLR and average MLR keep rising, and the linear fitting expression can be written as follows:

$$\dot{m}_1'' = 0.1046\dot{q}_e'' + 2.9438, \tag{3}$$

$$\dot{m}_2'' = 0.1395\dot{q}_e'' + 1.9543, \tag{4}$$

$$\dot{m}_a'' = 0.0771\dot{q}_e'' + 1.9256, \tag{5}$$

where $\dot{m}_1''$, $\dot{m}_2''$ and $\dot{m}_a''$ represent the first peak, second peak and average MLR of the sample, respectively.

Generally speaking, the thermal behaviors of materials change from thermally thick in the first phase to thermally thin in the last ones during the decomposition process. In this process, due to phase transition, carbonization, vaporization and other effects, the thermal properties of the material have undergone a complete change [19]. Therefore, the
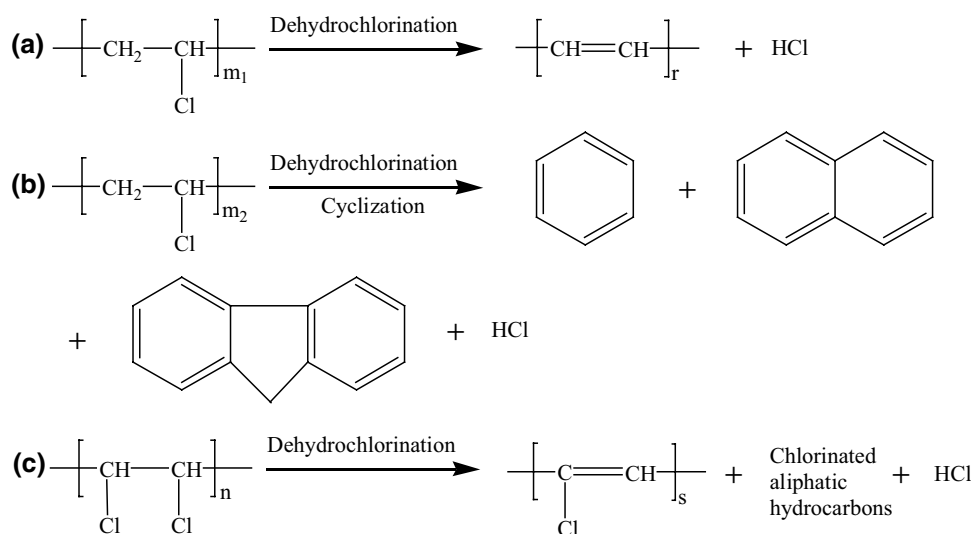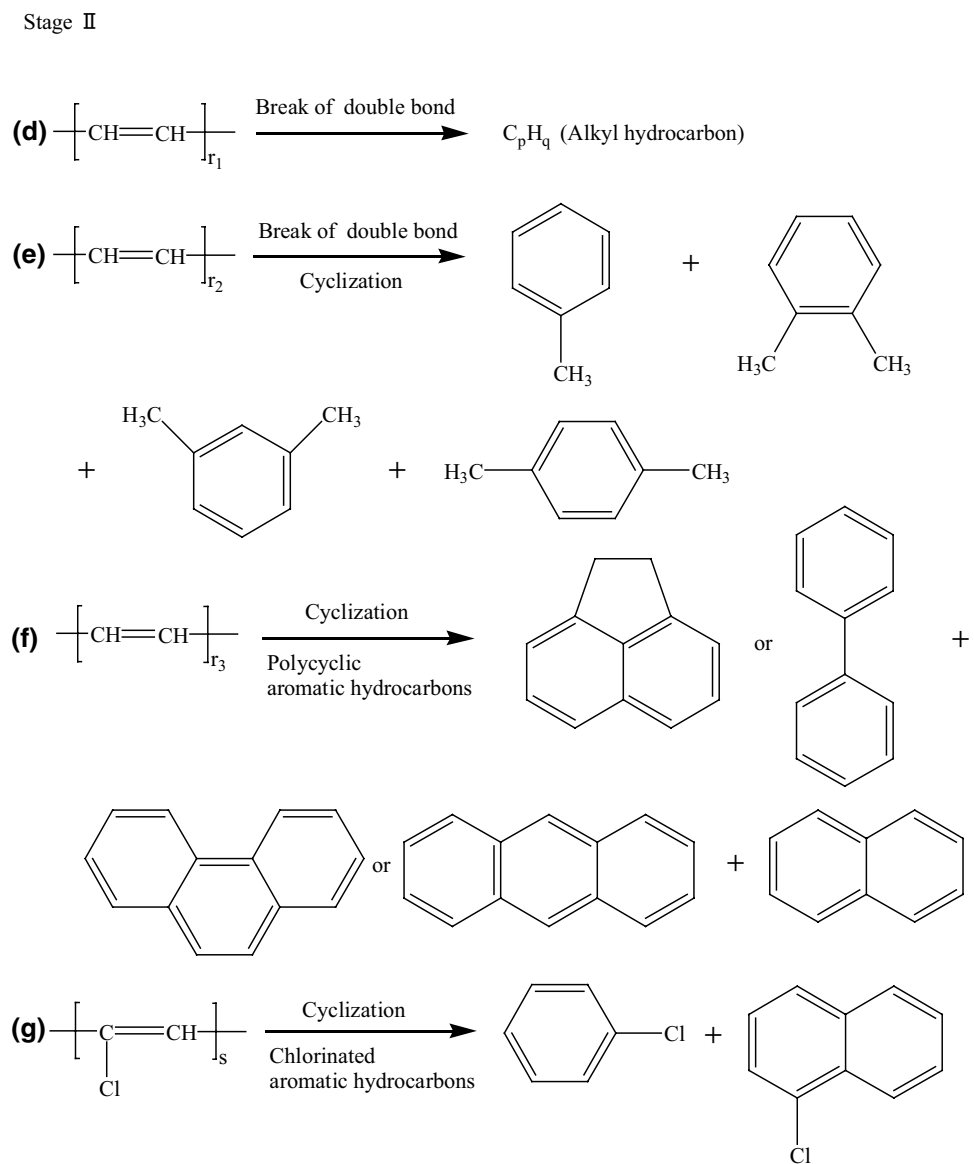
Fig. 4 Possible reactions of CPVC pyrolysis in Stage I

Fig. 5 Possible reactions of CPVC pyrolysis in Stage II

Stage II

average MLR as a function of external heat fluxes will lead to wrong value of the heat of gasification. Then the correlation coefficient of the first peak MLR against external heat flux is not high ($R^2 = 0.7046$), so the second peak MLR is selected to calculate the heat of gasification. Based on the slope of Eq. (2), the heat of gasification L can be calculated as 7.1666 kJ g^{-1}.

Heat release rate

HRR denotes the rate of thermal energy released from the combustion of the solid combustibles and is considered as the most important variable in fire hazard evaluation [34]. Figure 7a shows the HRR against time under four different external heat fluxes. Similar to MLR curves, there are also two peaks in the HRR curves.

Based on the references [35, 36], the transient value of HRR can be expressed by MLR and theoretical combustion heat:

$$\dot{q}'' = \dot{m}'' \Delta H_{\text{eff}} = \dot{m}'' \chi \Delta H_{\text{c,s}} = \frac{\Delta H_{\text{eff}}}{L}\left(\dot{q}_e'' + \dot{q}_{f,c}'' + \dot{q}_{f,r}'' - \dot{q}_{\text{cond}}'' - \sigma\left(T_V^4 - T_\infty^4\right)\right), \tag{6}$$
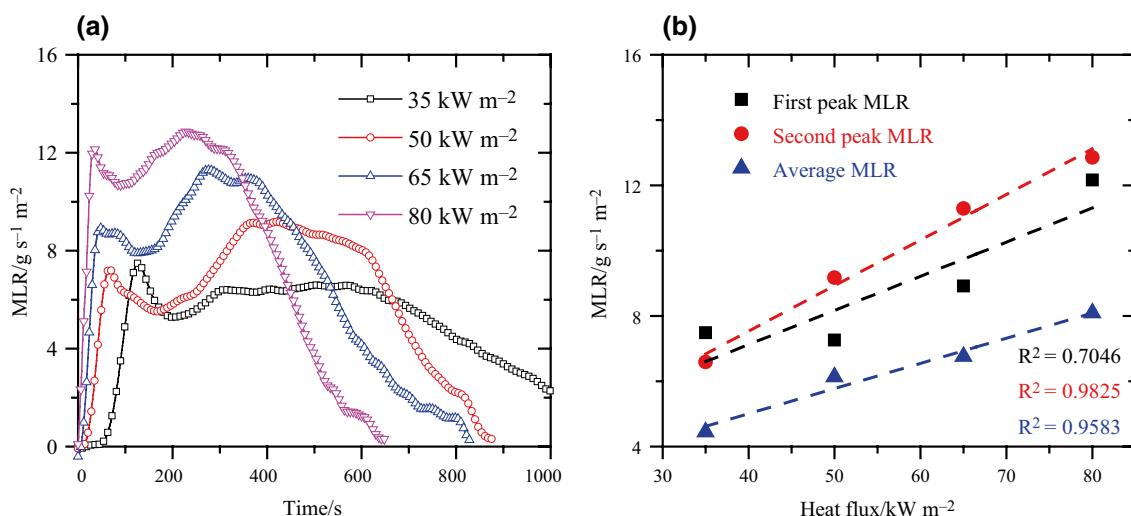
Fig. 6 **a** MLR at different external heat fluxes, and **b** MLR versus external heat flux

Table 3 Summary of MLR data

External heat flux/kW m^{-2}	PMLR$_1$/g s^{-1} m^{-2}	PMLR$_2$/g s^{-1} m^{-2}	AMLR/g s^{-1} m^{-2}
35	7.4861	6.5883	4.4447
50	7.2596	9.1724	6.1356
65	8.9172	11.2911	6.7571
80	12.1617	12.8589	8.0911

where $\dot{q}''$ represents the transient HRR, kW m^{-2}. χ is the combustion efficiency. ΔH_{eff} is the effective heat of combustion based on the evolved gas components, kJ g^{-1}. $\Delta H_{c,s}$ is the theoretical heat of combustion, kJ g^{-1}.

As demonstrated in Sect. 3.2.1, the peak and average MLRs can be linearly correlated with the external heat flux, and then HRR is proportional to the MLR with constant effective heat of combustion for a specific material according to Eq. (6). Thus, the HRR, just like the MLR, also have a linear relationship with the external heat flux:

$$\dot{q}'' = \dot{m}'' \Delta H_{\text{eff}} = \frac{\Delta H_{\text{eff}}}{L} \dot{q}_e'' + C_2, \tag{7}$$

where C_2 is a constant.

The first peak, second peak, and average HRR (PHRR$_1$, PHRR$_2$ and AHRR) values are listed in Table 4. Figure 7b shows the first, the second and the average HRR against external heat flux. It shows that all of them increase with the heat
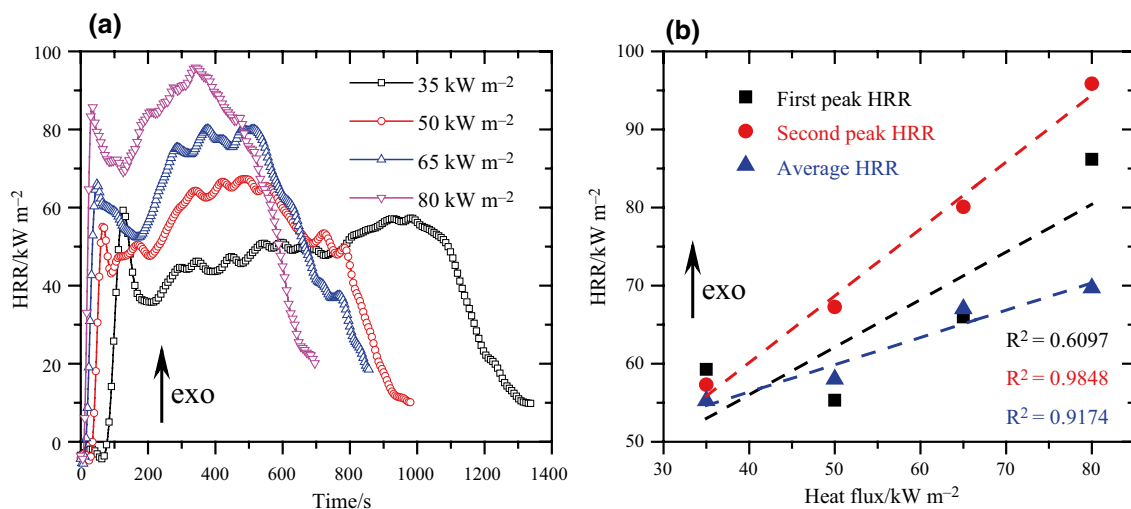

Fig. 7 **a** HRR at different external heat fluxes, and **b** HRR versus external heat flux

Table 4 Summary of HRR data

External heat flux/kW m^{-2}	PHRR$_1$/kW m^{-2}	PHRR$_2$/kW m^{-2}	AHRR/kW m^{-2}
35	59.2687	57.3046	55.2590
50	55.3278	67.2640	58.0075
65	65.9891	80.0862	67.0289
80	86.1842	95.8634	69.6915

flux, similar to the trend of MLR. The mathematical expression between them can be expressed as:

$$\dot{q}_1'' = 0.6049\dot{q}_e'' + 31.6528, \tag{8}$$

$$\dot{q}_2'' = 0.8567\dot{q}_e'' + 25.8718, \tag{9}$$

$$\dot{q}_a'' = 0.3488\dot{q}_e'' + 42.4412, \tag{10}$$

where $\dot{q}_1''$, $\dot{q}_2''$ and $\dot{q}_a''$ represent the first peak, second peak and average HRR of the sample, respectively.

The highest correlation coefficient ($R^2 = 0.9848$) among the three fitting relationships is the second peak versus

external heat flux. Based on MLR results, the second peak HRR is also selected to calculate the effective heat of combustion ($\Delta H_{eff} = 6.1393$ kJ g^{-1}) base on Eq. (7).

Fire performance index and fire growth index

To evaluate the fire safety better, two representative parameters FPI and FGI are be used to characterize. FPI can be used to evaluate the propensity to flashover in the whole fire process. High FPI value denotes large fire hazard. FGI usually represents the development rate of fire from the perspective of heat release. More detailed information about FPI and FGI is presented in Table 5. The values of FPI and FGI can be calculated by the following Eqs. (11) and (12):

$$FPI = PHRR/TTI, \tag{11}$$

$$FGI = PHRR/TTP, \tag{12}$$

where TTI and TTP are time to ignition, s, and time to PHRR, s, respectively. TTI, TTP$_1$ (time to PHRR corresponding to the first peak) and TTP$_2$ (time to PHRR corresponding to the second peak) values are listed in Table 5.

Table 5 Summary FPI and FGI data

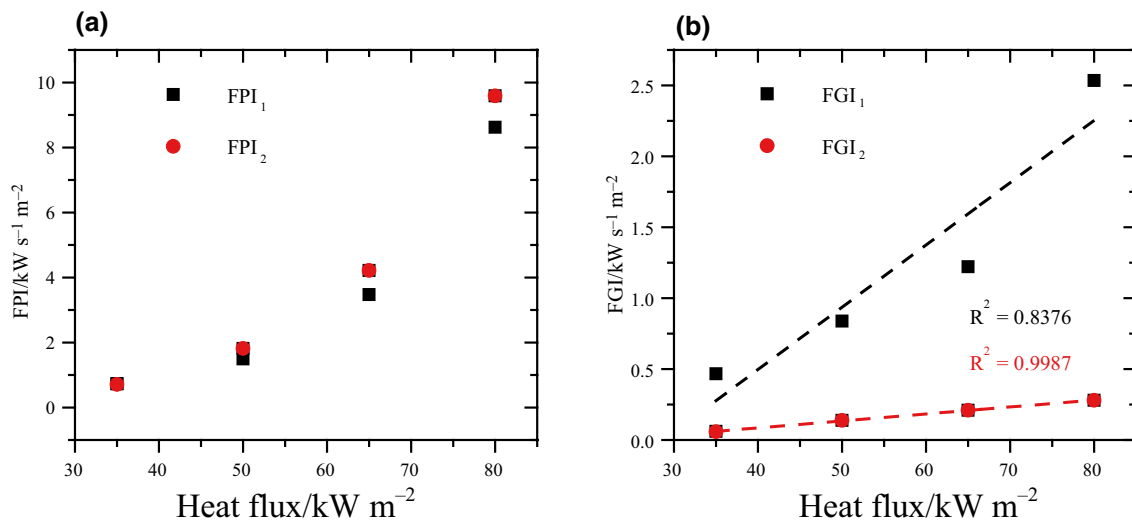| External heat flux/kW m^{-2}	TTI/s	TTP$_1$/s	TTP$_2$/s	FPI$_1$/kW s^{-1} m^{-2}	FPI$_2$/kW s^{-1} m^{-2}	FGI$_1$/kW s^{-1} m^{-2}	FGI$_2$/kW s^{-1} m^{-2}
35	81	127	982	0.7317	0.7075	0.4667	0.0584
50	37	66	486	1.4953	1.8179	0.8383	0.1384
65	19	54	383	3.4731	4.2151	1.2220	0.2091
80	10	34	342	8.6184	9.5863	2.5348	0.2803

Fig. 8 **a** FPI versus external heat flux, and **b** FGI versus external heat flux
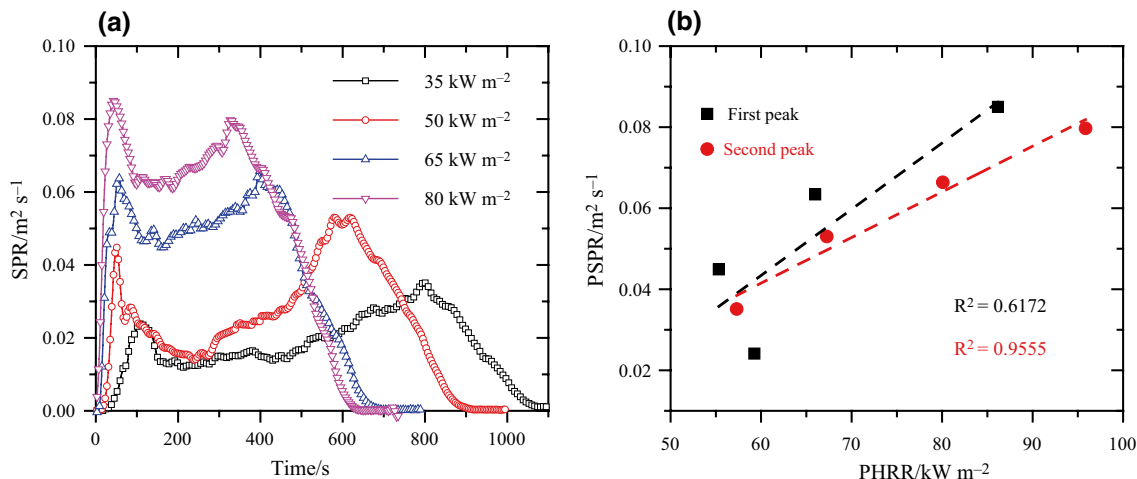
Fig. 9 **a** SPR against time under four external heat fluxes, and **b** PSPR vs. PHRR

Table 6 Summary of SPR data

External heat flux/kW m^{-2}	$PSPR_1/m^2\ s^{-1}$	$PSPR_2/m^2\ s^{-1}$
35	0.0241	0.0351
50	0.0449	0.053
65	0.0634	0.0664
80	0.085	0.0797

Figure 8a shows the first and second peaks FPI (FPI_1 and FPI_2) with the external heat flux, respectively. Both FPI_1 and FPI_2 increase gradually with the increase of external heat flux. The linear fitting relationship in the first and second peaks FGI (FGI_1 and FGI_2) with the external heat flux is shown Fig. 8b. Compared with FGI_1, FGI_2 has a higher correlation with external heat flux. It also showed that FGI_2 was more reliable in the characterization of CPVC fire risk.

Smoke and CO/CO_2 production rate

Except for MLR and HRR, SPR is also an important parameter to evaluate the fire safety of materials during combustion. Materials may produce poisonous and harmful gases in the process of pyrolysis and combustion, which will not only harm human life and health, but also pollute the environment. The variation of SPR with respect to time under four different heat fluxes is shown in Fig. 9a. It can be seen that the change of SPR curves are similar to that of HRR and MLR. The two peaks increase with the increase of the external heat flux. The first peak and second peak SPR ($PSPR_1$ and $PSPR_2$) values are listed in Table 6.
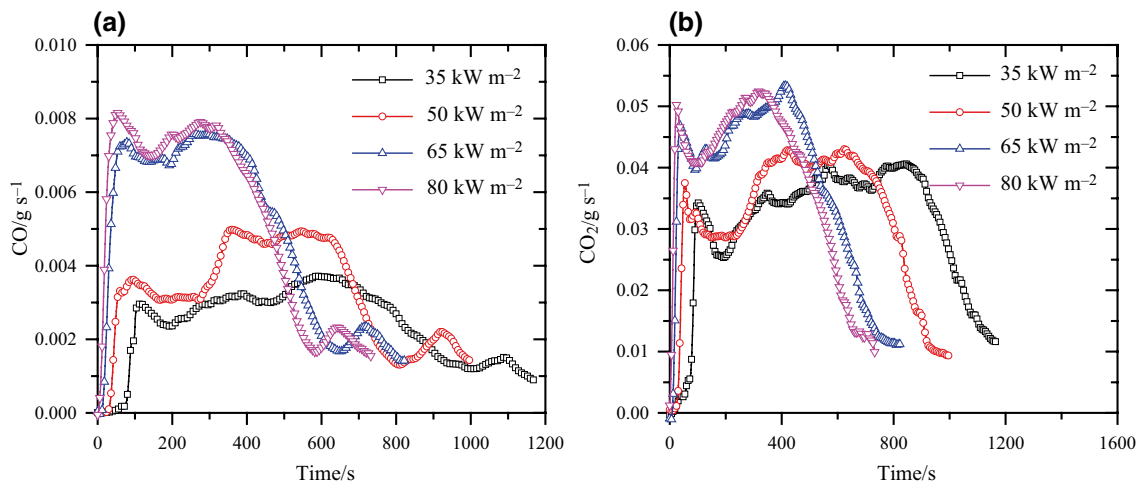

Fig. 10 CO and CO_2 production rate against time under four external heat fluxes: **a** CO, and **b** CO_2

The relationship between HRR and SPR of four decorative materials was studied by Xu et al. [37]. The results show that peak SPR and peak HRR have linear correlation. The positive correlation indicates that the material is combustible while the negative correlation is noncombustible. Taking into account the correlation between heat and smoke in material combustion, the first peak SPR versus the first peak HRR and the second peak SPR versus the second peak HRR are shown in Fig. 9b. It can be seen that the positive correlation between peak SPR and HRR. It also indicates that CPVC is combustible.

CO and CO_2, as the important toxic gas components involved in the smoke, are paid more attention in the fire risk. Figure 10 illustrates the CO and CO_2 production rate against time under four external heat fluxes. The variation trend of CO and CO_2 is similar, corresponding to SPR, while the value of production rate of CO_2 is almost ten times higher than that of CO.

Conclusions

TG–FTIR–MS were used to study the gas products of CPVC pyrolysis, which could be considered as two main stages (Stages I and II). By comparison with pyrolysis gas products of PVC, there were other chlorinated compounds of CPVC pyrolysis besides HCl in Stage I, and the gas products mainly consisted of homologues or derivatives of benzene and polycyclic aromatic compounds (xylene and ethylbenzene, chlorobenzene and 1-chloronaphthalene, naphthalene and fluorene and so on) in Stage II. The possible reactions during CPVC pyrolysis were put forward based on the results of TG–FTIR–MS.

Cone calorimeter experiments were conducted to explore the combustion properties and smoke production. The peaks of MLR, HRR and SPR appear earlier with the increase of the external heat flux. The second peak corresponding to MLR, HRR, FGI and SPR curves has a good correlation with the external heat flux. In addition, the positive correlation between peak SPR and peak HRR not only indicates that CPVC is a combustible material, but also shows there is a correlation between the heat release and smoke emission of CPVC during combustion. The variations of smoke and CO and CO_2 rate in the whole combustion process are similar. These results would be the important references for the fire risk.

Author contributions AL and BH were involved in the methodology, validation, data curation, and writing. WZ contributed to the methodology, and writing. YD was involved in the supervision, funding acquisition, project administration, and writing. RZ contributed to the data curation.

Declarations

Conflict of interest Not applicable.

References

1. Dayana ASS, Abnisa F, Ashri WDWM, Kheireddine AM. A review on pyrolysis of plastic wastes. Energy Convers Manag. 2016;115:308–26. https://doi.org/10.1016/j.enconman.2016.02.037.

2. An W, Jiang L, Sun J, Liew KM. Correlation analysis of sample thickness, heat flux, and cone calorimetry test data of polystyrene foam. J Therm Anal Calorim. 2015;119:229–38. https://doi.org/10.1007/s10973-014-4165-9.

3. Yang Q, Lu W, Bai L, Yan B, Cheng Y. UV enhanced gas–solid synthesis of chlorinated poly vinyl chloride characterized by a UV–Vis online analysis method. Chin J Chem Eng. 2015;23(6):1052–9. https://doi.org/10.1016/j.cjche.2014.12.002.

4. Zhang W, Zhang J, Ding Y, Zhou R, Mao S. The accuracy of multiple methods for estimating the reaction order of representative thermoplastic polymers waste for energy utilization. Energy. 2022;239B:122112. https://doi.org/10.1016/j.energy.2021.122112.

5. Zhang W, Zhang J, Ding Y, He Q, Lu K, Chen H. Pyrolysis kinetics and reaction mechanism of expandable polystyrene by multiple kinetics methods. J Clean Prod. 2021;285: 125042. https://doi.org/10.1016/j.jclepro.2020.125042.

6. Huang J, Li X, Zeng G, Cheng X, Tong H, Wang D. Thermal decomposition mechanisms of poly(vinyl chloride): a computational study. Waste Manag. 2018;76:483–96. https://doi.org/10.1016/j.wasman.2018.03.033.

7. Wu J, Chen T, Luo X, Han D, Wang Z, Wu J. TG/FTIR analysis on co-pyrolysis behavior of PE, PVC and PS. Waste Manag. 2014;34(3):676–82. https://doi.org/10.1016/j.wasman.2013.12.005.

8. Jin W, Shen D, Liu Q, Xiao R. Evaluation of the co-pyrolysis of lignin with plastic polymers by TG–FTIR and Py-GC/MS. Polym Degrad Stab. 2016;133:65–74. https://doi.org/10.1016/j.polymdegradstab.2016.08.001.

9. Zhou R, Huang B, Ding Y, Li W, Mu J. Thermal decomposition mechanism and kinetics study of plastic waste chlorinated polyvinyl chloride. Polymers. 2019. https://doi.org/10.3390/polym11122080.

10. Ding Y, Ezekoye OA, Zhang J, Wang C, Lu S. The effect of chemical reaction kinetic parameters on the bench-scale pyrolysis of lignocellulosic biomass. Fuels. 2018;232:147–53. https://doi.org/10.1016/j.fuel.2018.05.140.

11. Ding Y, Huang B, Li K, Du W, Lu K, Zhang Y. Thermal interaction analysis of isolated hemicellulose and cellulose by kinetic parameters during biomass pyrolysis. Energy. 2020;195: 117010. https://doi.org/10.1016/j.energy.2020.117010.

12. Kai X, Li R, Yang T, Shen S, Ji Q, Zhang T. Study on the co-pyrolysis of rice straw and high density polyethylene blends using

TG–FTIR–MS. Energy Convers Manag. 2017;146:20–33. https://doi.org/10.1016/j.enconman.2017.05.026.

13. Kai X, Yang T, Shen S, Li R. TG–FTIR–MS study of synergistic effects during co-pyrolysis of corn stalk and high-density polyethylene (HDPE). Energy Convers Manag. 2019;181:202–13. https://doi.org/10.1016/j.enconman.2018.11.065.

14. Chen R, Lu S, Zhang Y, Lo S. Pyrolysis study of waste cable hose with thermogravimetry/Fourier transform infrared/mass spectrometry analysis. Energy Convers Manag. 2017;153:83–92. https://doi.org/10.1016/j.enconman.2017.09.071.

15. Chen R, Xu X, Lu S, Zhang Y, Lo S. Pyrolysis study of waste phenolic fibre-reinforced plastic by thermogravimetry/Fourier transform infrared/mass spectrometry analysis. Energy Convers Manag. 2018;165:555–66. https://doi.org/10.1016/j.enconman.2018.03.092.

16. Gao X, Jiang L, Xu Q. Experimental and theoretical study on thermal kinetics and reactive mechanism of nitrocellulose pyrolysis by traditional multi kinetics and modeling reconstruction. J Hazard Mater. 2020;386: 121645. https://doi.org/10.1016/j.jhazmat.2019.121645.

17. Luche J, Rogaume T, Richard F, Guillaume E. Characterization of thermal properties and analysis of combustion behavior of PMMA in a cone calorimeter. Fire Saf J. 2011;46(7):451–61. https://doi.org/10.1016/j.firesaf.2011.07.005.

18. Luche J, Mathis E, Rogaume T, Richard F, Guillaume E. High-density polyethylene thermal degradation and gaseous compound evolution in a cone calorimeter. Fire Saf J. 2012;54:24–35. https://doi.org/10.1016/j.firesaf.2012.08.002.

19. Quang Dao D, Luche J, Richard F, Rogaume T, Bourhy-Weber C, Ruban S. Determination of characteristic parameters for the thermal decomposition of epoxy resin/carbon fibre composites in cone calorimeter. Int J Hydrog Energy. 2013;38(19):8167–78. https://doi.org/10.1016/j.ijhydene.2012.05.116.

20. Qu H, Liu C, Wu W, Chen L, Xu J. Using cone calorimeter to study thermal degradation of flexible PVC filled with zinc ferrite and $Mg(OH)_2$. J Therm Anal Calorim. 2014;115:1081–7. https://doi.org/10.1007/s10973-013-3434-3.

21. Bai X, Wang Q, Sui S, Zhang C. The effects of wood-flour on combustion and thermal degradation behaviors of PVC in wood-flour/poly(vinyl chloride) composites. J Anal Appl Pyrolysis. 2011;91(1):34–9. https://doi.org/10.1016/j.jaap.2011.02.009.

22. IS0-5660-1. Reaction-to-fire tests-heat release, smoke production and mass loss rate—Part 1 heat release rate (cone calorimeter method). Switzerland; 2002.

23. Srivastav V, Sabarilal S, Kumar A. Numerical study on sample thickness dependence of fire response properties of polymeric materials (charring and non-charring) in standard cone calorimeter test. In: Gupta A, Mongia H, Chandna P, Sachdeva G, editors. Advances in IC engines and combustion technology. NCICEC 2019. Lecture notes in mechanical engineering. Singapore: Springer. https://doi.org/10.1007/978-981-15-5996-9_71.

24. Özsin G, Pütün AE. TGA/MS/FT-IR study for kinetic evaluation and evolved gas analysis of a biomass/PVC co-pyrolysis process. Energy Convers Manag. 2019;182:143–53. https://doi.org/10.1016/j.enconman.2018.12.060.

25. Xu F, Wang B, Yang D, Hao J, Qiao Y, Tian Y. Thermal degradation of typical plastics under high heating rate conditions by TG–FTIR: pyrolysis behaviors and kinetic analysis. Energy Convers Manag. 2018;171:1106–15. https://doi.org/10.1016/j.enconman.2018.06.047.

26. Soudais Y, Moga L, Blazek J, Lemort F. Coupled DTA–TGA–FT-IR investigation of pyrolytic decomposition of EVA, PVC and cellulose. J Anal Appl Pyrolysis. 2007;78(1):46–57. https://doi.org/10.1016/j.jaap.2006.04.005.

27. Zhu HM, Jiang XG, Yan JH, Chi Y, Cen KF. TG–FTIR analysis of PVC thermal degradation and HCl removal. J Anal Appl Pyrolysis. 2008;82(1):1–9. https://doi.org/10.1016/j.jaap.2007.11.011.

28. Zhou H, Meng A, Long Y, Li Q, Zhang Y. Interactions of municipal solid waste components during pyrolysis: a TG–FTIR study. J Anal Appl Pyrolysis. 2014;108:19–25. https://doi.org/10.1016/j.jaap.2014.05.024.

29. Sun Q, Shi X, Lin Y, Zhu H, Wang X, Cheng C, et al. Thermogravimetric–mass spectrometric study of the pyrolysis behavior of PVC. J China Univ Min Technol. 2007;17(2):242–5. https://doi.org/10.1016/s1006-1266(07)60080-7.

30. Knümann R, Bockhorn H. Investigation of the kinetics of pyrolysis of PVC by TG–MS-analysis. Combust Sci Technol. 1994;101(1–6):285–99. https://doi.org/10.1080/00102209408951877.

31. Huang L. Production and application of chlorinated PVC resins. Polyvinyl Chloride. 2002;1:15–20 (**in Chinese**).

32. Rhodes BT, Quintiere GJ. Burning rate and flame heat flux for PMMA in a cone calorimeter. Fire Saf J. 1996;26(3):221–40. https://doi.org/10.1016/S0379-7112(96)00025-2.

33. Chen R, Lu S, Li C, Ding Y, Zhang B, Lo S. Correlation analysis of heat flux and cone calorimeter test data of commercial flame-retardant ethylene–propylene-diene monomer (EPDM) rubber. J Therm Anal Calorim. 2015;123(1):545–56. https://doi.org/10.1007/s10973-015-4900-x.

34. Chen R, Xu X, Zhang Y, Lu S, Lo S. Characterization of ignition and combustion characteristics of phenolic fiber-reinforced plastic with different thicknesses. J Therm Anal Calorim. 2019;140(2):645–55. https://doi.org/10.1007/s10973-019-08903-4.

35. Ding Y, Fukumoto K, Ezekoye OA, Lu S, Wang C, Li C. Experimental and numerical simulation of multi-component combustion of typical charring material. Combust Flame. 2020;211:417–29. https://doi.org/10.1016/j.combustflame.2019.10.016.

36. Zhang Z, Wang C, Huang G, Liu H, Zhao W. Thermal decomposition characteristic parameters for the outer material of composite hydrogen storage tank by cone calorimeter. J Therm Anal Calorim. 2019;138(2):1299–310. https://doi.org/10.1007/s10973-019-08189-6.

37. Xu Z, Yan L, Liu Y. Study on Correlations between the flammability and dynamic smoke properties of four decorative materials. Procedia Eng. 2014;84:498–505. https://doi.org/10.1016/j.proeng.2014.10.461.